Capacitance spectroscopy of thin-film formamidinium lead lodide based perovskite solar cells

A. Urbaniak, A. Czudek, J. Dagar, E. L. Unger

[1]Faculty of Physics, Warsaw University of Technology, Koszykowa 75, PL 00662 Warsaw, Poland

[2]Helmholtz-Zentrum Berlin für Materialien und Energie GmbH, Forschergruppe Generative Fertigungsprozesse, Hahn-Meitner-Platz 1, Berlin, 14109, Germany

Abstract

This work concerns the interpretation of capacitance spectroscopy results in perovskite-based solar cells. Based on the deep level transient spectroscopy and admittance spectroscopy results, we present arguments that the observable signals in perovskite-based solar cells come from anion migration rather than being a response from deep trap energy levels. The ion migration parameters, such as activation energy and ion concentration, are calculated and compared to theoretical values for different migration paths of ions in perovskites. Those parameters evolve with time, reflecting in the degradation of the cells, which we propose to link with a change in the anion migration path in perovskite.

1. Introduction

Solar cells using perovskite materials are currently the fastest growing photovoltaic technology, reaching record efficiencies exceeding 25 %[1]. Their unique properties, such as long charge carrier diffusion lengths [2], high mobility of charge carriers [3], high absorption coefficient [4], and low exciton binding energy [5], allow perovskite-based solar cells (PSCs) to convert solar energy into electricity very efficiently. To fully exploit the potential of perovskite materials in photovoltaics, it is essential to know and understand the physical mechanisms affecting a solar cell's performance. One of the critical areas regarding solar cell efficiency is the physics of defects in the device – their type, parameters, and their role in the solar cell. In optoelectronic devices, deep energy levels in the energy gap are introduced by defects, which can act as recombination centers that reduce the minority charge carrier lifetime. In solar cells, the presence of deep defect levels reduces the number of photogenerated electrons, which affects the photovoltaic parameters of a solar cell, such as open-circuit voltage, fill factor, and efficiency.

Capacitance-based techniques such as admittance spectroscopy (AS) [6] and deep level transient spectroscopy (DLTS) [7] are commonly used to investigate defects in solar cells. They allow for the determination of the electrical parameters of defects, such as the capture and thermal emission rates of charge carriers, the activation energy of these processes, their cross-section, and the defect concentration. These techniques have been used to investigate

defects in various types of semiconductor thin-film solar cells, i.e., in a-Si [8], Cu(In,Ga)Se_2 [9], or CdTe [10] – based devices. However, the use of capacitance spectroscopy techniques in perovskite solar cells is not as straightforward as in the case of inorganic thin-film solar cells. The theory of both AS and DLTS utilizes the concept of a space charge region and so-called depletion approximation. According to this, the space charge region is depleted from free charge carriers. This assumption is not fulfilled in perovskite solar cells, as they are mixed ionic-electronic conductors [11], and slow-moving ions are present in the space charge region. However, this does not limit the use of capacitance spectroscopy methods in PSCs, as those techniques can also be applied to quantify processes related to ion diffusion or electromigration.

Ion diffusion is linked to another vital research area on perovskite cells – their stability and degradation over time. One of the routes to improve stability of perovskite-based devices is to make a mixed cation and mixed anion materials including most of the (MA,FA,Cs) cation with (I,Br,Cl) combinations i.e. (MA,FA)PbI_3 [12], (Cs,FA)$Pb(I,Br)_3$ [13],[14] or Cs(M,Fa)$Pb(I,Cl)_3$ [15]. Mobile ions and related ionic defects have already been linked to current-voltage hysteresis and reduced stability of perovskite-based solar cells [16][17] and investigated using capacitance spectroscopy techniques. The interpretation of the capacitance spectroscopy results follows two paths. The observable signals are considered either to appear as a response from deep energy levels introduced by defects in the bulk of a perovskite material [18][19] or be related to the diffusion of mobile ions [20][21][22]. Theoretical works support both the existence of native point defects in perovskites such as V_I^+ and V_{MA}^- vacancies as well as I_i^- and MA_i^+ interstitials [23][24] as well as mechanisms of diffusion in perovskite-based solar cells [21][25][26].

In this work, we discuss the results of AS and DLTS for perovskite cells based on formamidinium lead iodide ($FAPbI_3$). Using a modified DLTS procedure we were able to present arguments that the results of capacitance spectroscopy techniques relate to the ion diffusion parameters rather than electron or hole thermal emission from defect energy levels and calculate activation energies of the observed processes. We discussed the obtained results in the light of other research on solar cells using other perovskite materials, showing that the observed processes are universal for various perovskite materials. We observed that the activation energy of the observed processes decreases with time and correlating with the progressive degradation of the cell.

2. Experimental methods

2.1 Perovskite solar cell fabrication

P-i-n planar perovskite solar cells with a layer configuration of ITO/2PACz/$Cs_{0.15}FA_{0.85}PbI_{2.7}Br_{0.3}$/$C_{60}$/$SnO_2$/Cu were fabricated using the following procedure: First, 25 x 25 mm patterned glass/ITO substrates with a resistivity of 15 Ω sq^{-1} were cleaned sequentially according to a procedure described previously [27][28]. Next, a 1 mmol 2PACz ([2-(9H-carbazol-9-yl)ethyl]phosphonic acid) solution was prepared by dissolving the

precursor in anhydrous ethanol and spin-coated onto a cleaned ITO substrate at a speed of 3000 rpm for 30 s, followed by annealing at 100 °C for 10 minutes. FACs perovskite ink was prepared by dissolving PbI_2 (446.4 mg), $PbBr_2$ (121.6 mg), FAI (185.5 mg), and CsI (57.4 mg) precursors in 0.750 ml dimethylformamide (DMF) and 0.250 ml dimethyl sulfoxide (DMSO) in a single vial. The vial was held on a shaker for 2 h at 60 °C. FACs perovskite ink was filtered using a 0.2 µm sized polytetrafluoroethylene filter before use.
A perovskite layer was spin-coated onto ITO/2PACz substrates with a spin speed of 3500 rpm for a 40 s steady duration. 250 µl anisole was dropped on the perovskite wetted spinning film 10 s before it was finished. The substrates were immediately annealed at 100 °C for 30 min. in an inert atmosphere.

In the evaporation chamber, C_{60} (23 nm) was thermally evaporated on the perovskite layer followed by the deposition of a SnO_2 (20 nm) layer by performing an atomic layer deposition technique using an Arradiance GEMStar reactor via applying 140 cycles at a substrate temperature of 80 °C. As top electrodes, Cu of 100 nm thickness was thermally deposited at a base pressure of 10^{-6} mbar. The active area of a solar cell is calculated to be 0.16 cm^2, as determined by microscopic imaging. The standard *J–V* measurements of PSCs were carried out under under Standard Test Conditions (Air Mass 1.5G spectrum and 1000 W m^{-2} light intensity) using a sun simulator of class AAA calibrated with a silicon reference cell (Fraunhofer ISE) according to a procedure described previously [29]. The mean photovoltaic parameters of the investigated PSCs are listed in Table 1.

Table 1. Mean values of the photovoltaic parameters of the investigated solar cells.

J_{SC} (mA/cm^2)	22.1
V_{OC} [V]	1.07
FF [%]	74.5
efficiency [%]	17.7

The admittance measurements were made with an Agilent 4285A LCR meter by measuring capacitance as a function of ac voltage in a 100 Hz - 1 MHz frequency range at different temperatures, stabilized to 0.1 K. The DLTS measurements were made using a Bontoon 7200 capacitance bridge in a homemade setup wit DAQ card. The sampling frequency at which capacitance transients were collected was 50 kHz and the pulse length was 50 ms. The procedure used in the DLTS measurement was different from that of most other studies. Standard DLTS measurements take successive, multiple measurements of capacitance transients at one temperature, average them, and automatically calculate DLTS spectrum. This approach might not give proper results when slow processes take place and startring point of each transient is slightly different. In this work we recorded single capacitance transient at each temperature using a setup adapted with a homemade noise filter.

The samples were mounted in a closed-cycle helium cryostat, which allowed measurements in the 30 K to 360 K temperature range.

2.2 Admittance spectroscopy

Admittance spectroscopy is mainly used to characterize defects in semiconductor junctions and has been frequently applied to thin-film solar cells. It utilizes the fact that the thermally dependent charge carrier capture and emission processes can be described by a characteristic time constant and related to it frequency – a thermal capture or emission rate. If a thermal emission rate is higher than the frequency of the applied oscillating voltage, the emitted charge carriers will contribute to the capacitance leading to its increase. In the opposite situation, when the voltage oscillations are faster than the emission rate, which describes the observable process, it will not change the device's capacitance.

The case of electronic states introduced within the bandgap by defects, capture, and emission of charge carriers is described by SRH statistics [30]. The thermal emission rate describes those processes according to the following Equation:

$$e_T = N_{C,V} v_{th} \sigma_{e,h} exp\left(-\frac{E_T}{k_B T}\right) \quad (1)$$

where e_T is the thermal emission rate, $N_{C,V}$ is the density of states in a conduction or valence band, $\sigma_{e,h}$ is the electron or hole capture cross-section, v_{th} is the thermal velocity of charge carriers, k_B is the Boltzmann constant, and E_T is the trap activation energy. The density of states is proportional to $T^{3/2,}$ and the charge carriers' thermal velocity is proportional to $T^{1/2}$. Therefore, a T^2 factor is usually excluded from the preexponential factor in Equation (1). However, this can only be done when the observable process relates to the thermal emission from a defect level. The eT/T^2 plot versus 1/T is called an Arrhenius plot and allows trap parameters, such as E_T and $\sigma_{e,h}$, to be calculated.

A similar approach can be applied to many thermally activated processes involving charge carriers, such as excitation over a potential barrier [31] or activation of mobility in a defected material [32]. Furthermore, the frequency-dependent change of capacitance may arise due to ion migration [33], which may be the case in perovskite-based solar cells, as suggested in [34].

Due to the different work functions of contacts in perovskite solar cells, an internal electric field arises in the perovskite layer. If mobile ions are present in the material, they may accumulate at the contact interface – the anions drift to the ETL layer, and cations drift to the HTL layer. A schematic diagram indicating the influence of ion drift on the band diagram of a perovskite device is shown in Figure 1.

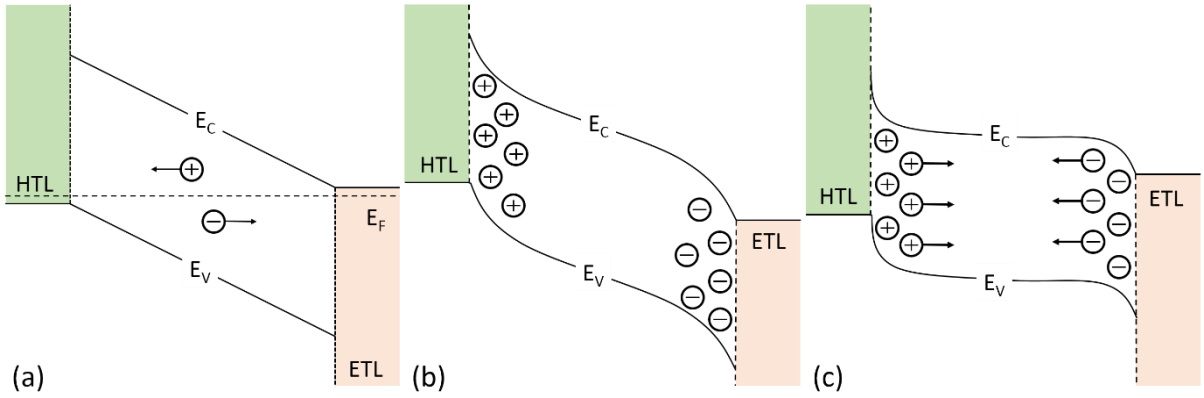

Figure 1. Schematic diagram of the influence of ion migration on the band diagram of a simplified perovskite solar cell. (a) at short circuit conditions (V = 0), the ions diffuse, anions towards the HTL layer, and cations toward the ETL layer, resulting in (b) an ion accumulation at the interface and the corresponding band bending. (c) when applying a voltage in the forward direction (V = V_0), mobile ions drift towards the bulk.

Then, the application of oscillating voltage leads to the migration of mobile ions with a time constant:

$$\tau = \frac{L^2}{D} = \frac{\varepsilon\varepsilon_0 k_B T}{q^2 N D} \tag{2}$$

where L is the diffusion length, ε_0 is the dielectric constant, ε_r is the relative dielectric permittivity of a material, q is the elementary charge, and N is the doping concentration. It is assumed here that mobile ion diffusion occurs only within the Debye length from the interface. However, it should be noted that it has also been suggested that ion migration in perovskites extends through the whole perovskite layer [25]. In a classical picture, where diffusion is described as a series of ionic jumps at some distance, the diffusion coefficient is expressed as [35]:

$$D = \frac{v_0 d^2}{6} exp\left(\frac{\Delta S}{k}\right) exp\left(-\frac{\Delta H}{k_B T}\right) \tag{3}$$

where v_0 is the attempt frequency of an ionic jump at a distance d, ΔS is the entropy change, and ΔH is the enthalpy change during an ionic jump. The attempt frequency v_0 is a vibration frequency of an attempt to break or loosen a bond, allowing a mobile ion to move to a new position. Assuming v_0 is independent of temperature, Equation (3) simplifies to an exponential relation of diffusion coefficient on 1/T:

$$D = D_0 exp\left(-\frac{\Delta H}{k_B T}\right) \tag{4}$$

Combining Equations (2) and (4), we obtain an Arrhenius relation for the ion migration rate that is similar to Equation (1):

$$\frac{1}{\tau} = \frac{q^2 N D_0}{\varepsilon \varepsilon_0 k_B T} exp\left(-\frac{\Delta H}{k_B T}\right) \quad (5)$$

2.3 DLTS

Deep level transient spectroscopy (DLTS) is another method used in defect characterization based on the device's capacitance. In this case, capacitance is measured in the time domain, not in the frequency domain as in the AS. However, the investigated processes are the same in both techniques. In a standard DLTS experiment, the negative voltage is applied to extend the space charge region in the device. The capacitance at the reverse bias V is then approximated by:

$$C = \frac{\varepsilon \varepsilon_0 A}{W} = A\sqrt{\frac{q\varepsilon_0 \varepsilon N}{2(V_{bi} - V)}} \quad (6)$$

where W is the space charge region width, A is the area of the device, and V_{bi} is the built-in potential. At the reverse voltage, the space charge region's traps are emptied. Applying the forward bias pulse narrows the space charge region, resulting in the capture of the majority of the carriers. The capture process is usually very fast and is described by the capture rate, which is proportional to the doping concentration N:

$$c_{e,h} = N\sigma_{e,h}\nu_{th} \quad (7)$$

Therefore, it is typically enough if the pulse length is on the order of milliseconds to fill the traps completely. After the pulse is removed, the trapped charge carriers are emitted and swept by the electric field. The emission process follows Equation (1) and is usually orders of magnitude slower than the capture process. Numerical analysis of capacitance transients allows for calculating the emission time constant and making the Arrhenius plot according to Equation (1) to obtain a defect level's activation energy. One method to get the time constant of a capacitance transient is a box-car analysis [36] made for different rate windows. It results in a temperature-dependent spectrum having an extremum when the rate window matches the emission rate at a specific temperature. Depending on what type of charge carriers are emitted, the transient is either decaying, the spectrum has a maximum for minority carriers or the capacitance increases, and the minimum is observed in the case of majority charge carriers.

The capacitance transient may arise not only due to the emission of charge carriers from traps but also from mobile ion drift. However, to obtain the ionic drift parameters, voltage biasing is different than in the case of traps. When the applied forward voltage is high enough, the space charge region entirely collapses. The mobile ions accumulated at the interface can now diffuse back to the perovskite layer (Figure 1c). This process will change the capacitance orders

of magnitude slower than in the case of charge carrier capture by traps. After removing the bias, the depletion region quickly returns, but due to the accumulation of ions during a forward bias pulse, its width is different from the initial one. The charge concentration that was previously equal to the doping concentration N now changes to $N \pm N_{ion}$ when N_{ion} is the density of mobile ions leading to different space charge regions and, thus, the different capacitance, according to Equation 6. After removing the forward bias pulse, the capacitance will return to the initial value with the time constant described by Equation 2. The corresponding capacitance transient can be analyzed in the same manner as in the trap response to obtain characteristic time constants, rates, and activation energy E_a being equal to enthalpy change (ΔH) during an ionic jump.

3. Results

An example of a series of admittance spectra at different temperatures for an investigated perovskite solar cell is presented in Figure 2. A step-like behavior of the capacitance spectrum between low and high ac voltage frequency is a fingerprint of a frequency-dependent process involving charge redistribution. The step in the admittance spectrum starts to be visible at around room temperature and evolves with the temperature as expected for the temperature-dependent process described by Equation 1. The phase angle of the device impedance was close to -90 ^{o} in the medium frequency range, indicating that the impedance's capacitance dominates in this regime. The phase angle was significantly lower in the low-frequency range where the C-f spectrum step was present, suggesting that the sample's resistivity also depends on the voltage frequency. Considering that the observable changes depend on the temperature, it might indicate that the physical process behind the admittance spectrum step's is somewhat related to ionic migration than to emission from traps, as it changes the device's resistance, not only its capacitance. At high frequencies, the real part of the impedance is also significant, with the phase angle lower than -90 ^{o}. However, the drop in capacitance at high frequencies does not depend on the temperature and seems to be related to the series resistance of the device.

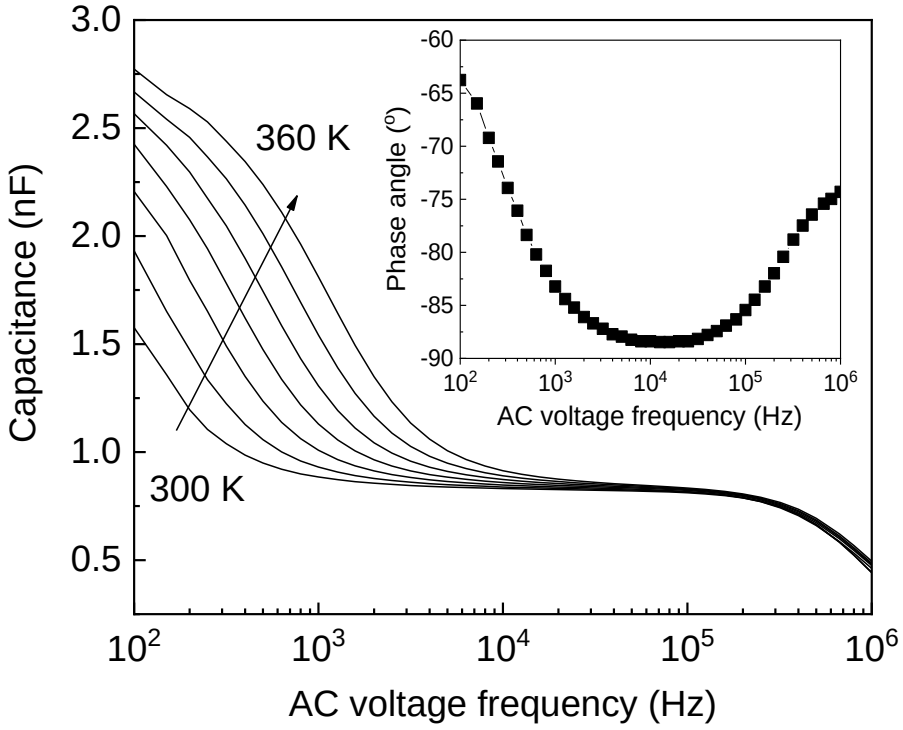

Figure 2. Admittance spectra for an investigated perovskite solar cell in the 300–360 K temperature range. Arrows indicate the step in capacitance between low and high ac voltage frequencies and its evolution with temperature. The insets show the impedance phase angle.

To get a deeper insight into whether the admittance signals are related to the deep traps or mobile ions, DLTS was applied. No transient was observed in a standard DLTS mode where the device is reverse biased, and no forward voltage pulse is applied. However, a large positive capacitance transient appeared when a +1 V voltage was applied onto an un-biased device. When the pulse was removed, the capacitance quickly dropped and then slowly decayed to the initial value. The capacitance transients measured at different temperatures are presented in Figure 3. The time frames of the experimental processes are, in both cases, up to tens of milliseconds, which is an expected value in both charge carrier emission from deep traps and ion migration. However, the capture of charge carriers at +1 V by a deep trap is expected to be orders of magnitude faster (for typical values of $N = 10^{16}$ cm^{-3}, $N\sigma_{e,h} = 10^{-14}$ cm^2, and $v_{th} = 10^7$ cm/s, the capture time constant equals 10 ns, see Equation 7).

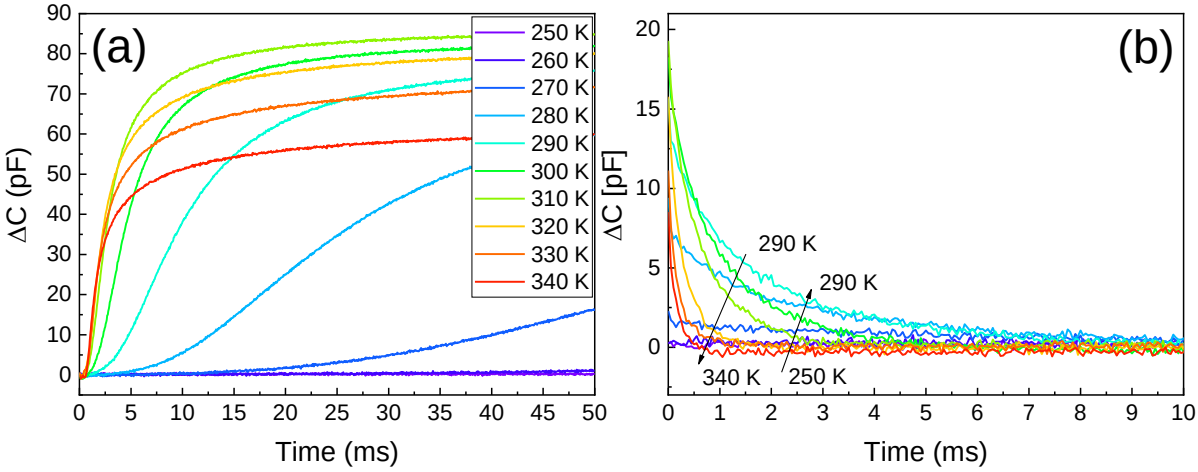

Figure 3. Capacitance transients arising (a) upon stepping from 0V to +1 V, measured at +1 V and (b) at 0 V after removing the +1 V pulse.

Capacitance kinetics were analyzed using the box-car algorithm. The calculated DLTS spectra are presented in Figure 4. The DLTS signal after the +1 V bias pulse was removed, measured when the space charge region is extended through the perovskite layer, is positive, which corresponds to the decay in the capacitance. Considering the observation of large capacitance transients at +1 V with a time constant of around 10 ms at room temperature, we interpret the observed signals as a result of ion migration rather than a deep trap response.

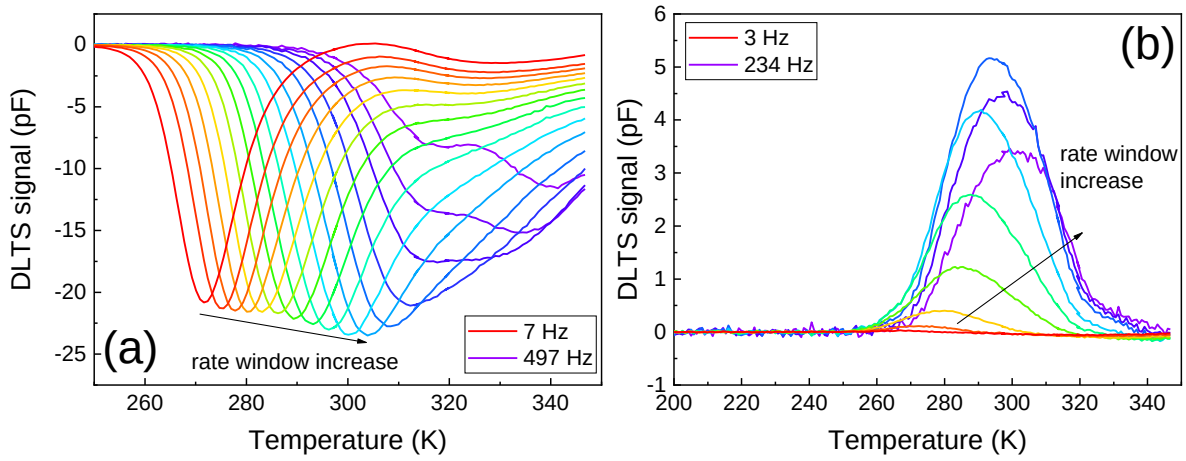

Figure 4. DLTS spectra calculated from the capacitance transients measured at (a) +1 V and (b) at 0 V after applying a +1 V pulse.

An Arrhenius plot of admittance and DLTS spectra is presented in Figure 5, along with the calculated activation energies. The thermal emission rates are plotted undivided by T^2, as this factor can only be excluded from Equation (1) in the case of emission from deep traps and is not present in Equation (5). The primary signal responsible for an admittance step shown in Figure 2 has an activation energy of around 0.45 eV. The same signal is observed in DLTS, at +1 V and 0 V. It has slightly higher activation energy. Still, it is a continuation of the admittance data on the Arrhenius plot. The different activation energy might also partially result from the distortion in the DLTS spectra introduced by a second peak appearing above room

temperature. An additional process with an activation energy of around 1.2 eV was observed in the capacitance transients measured at 0 V, but it was not related to the admittance signal.

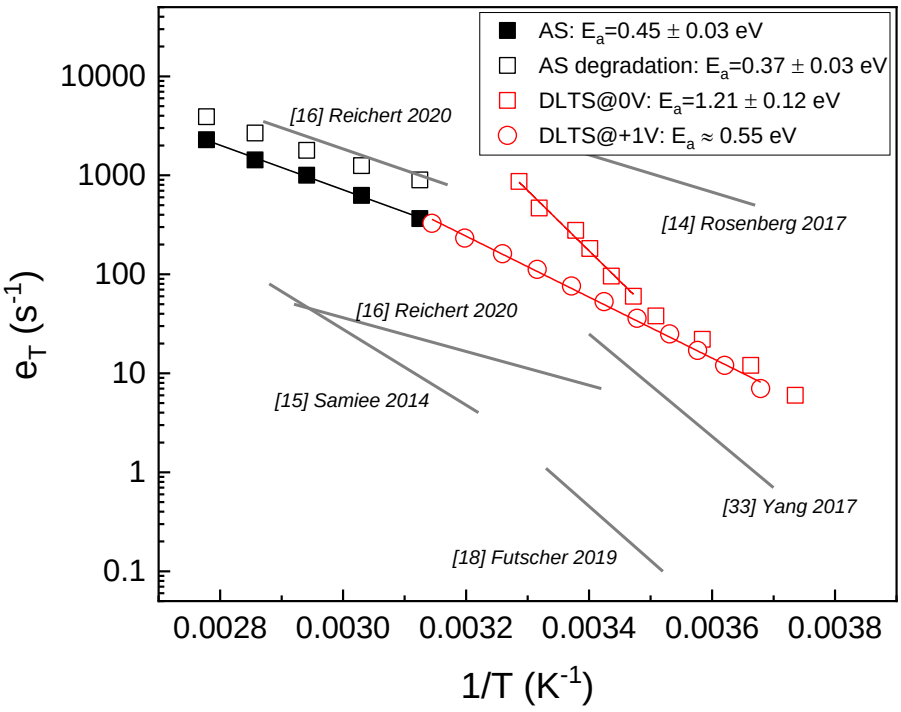

Figure 5. The Arrhenius plots of AS and DLTS data. Fitting lines to the migration and emission rates data reported in the literature [18] [19][20] [22][37], which place in a similar region as our date on the Arrhenius plot, are added for comparison with our results.

To evaluate our AS and DLTS results in light of other emission and migration rates results, we compared the Arrhenius plots obtained herein with available in the literature data on different perovskite-based devices. We restricted ourselves to the region of time constants and temperatures close to our results. A more complete collection of reported in the literature Arrhenius plots was presented by Reichert et al. [20]. Included in Figure 5 are the results of Rosenberg et al. [18], who observed two energy levels and attributed them to defects in $MAPbBr_3$ single crystals and Yang et al. [37] attributing the DLTS results on $FAPbI_3$ to FA^+ cations. Additionally, we have added the results of Samiee et al. [19] on mixed halide perovskites, Reichert et al. [20], and Futscher et al. [22] on $MAPbI_3$, all attributing observable signals to either to I^- or MA^+ migration. This comparison shows that apart from differences in emission/migration rates and activation energies, the results can be divided into two groups independently of the perovskite material investigated. The first group exhibit activation energies below 0.55 eV (AS and DLTS results presented herein, [18][20]), while the activation energies in the second group are significantly above 1 eV (part of our DLTS results, [19][22][37]). This assessment indicated at least two dominant mechanisms observed in PSC, universal for different perovskite materials used, which can tentatively be attributed to anion (low energies) and cation (high energies) migration.

The parameters of the admittance signals evolve with time. Between measurements, the samples were stored in ambient air in the dark. After approximately four months of storage (121 days), the activation energy decreased to 0.37 eV. Moreover, the height of the AS step decreased. This can be related to the reduced number of migrating ions, as the height of the admittance step is proportional to the ratio of the ion and doping concentration, respectively, according to:

$$\frac{\Delta C}{C_\infty} \approx \frac{N_{ion}}{2N} \tag{7}$$

where C_∞ is the capacitance at a high AC voltage frequency (100 kHz in this case). The doping concentration N was measured using the Drive Level Capacitance Profiling (DLCP) [38], a variation of a CV characterization – typical for doping measurements. The advantage of this technique is that it excludes the impact of slow processes, responding to the DC bias sweep during the measurement, which might be an ion migration in the case of perovskites. The doping concentration was (1.00 ± 0.35)*10^{15} cm^{-3}, which allowed to estimate the concentration of migrating ions responsible for the admittance step. After approximately four months, the estimated mobile ion concentrations decayed with time, from around 6.5*10^{15} cm^{-3} to 4.5*10^{15} cm^{-3}. The results are presented in Figure 6. Along with lowering the admittance step's height, the shunt resistance also decayed, from around 1.75 kΩ down to about 250 Ω, after the same time. The hypothesis that those two phenomena are related allows us to estimate the mobility of the migrating ions and how it evolves with time (inset in Figure 6). Even though the mobile ion concentration decays with time, suggesting lower sample conductivity, their mobility increases, resulting in a lower shunt resistance.

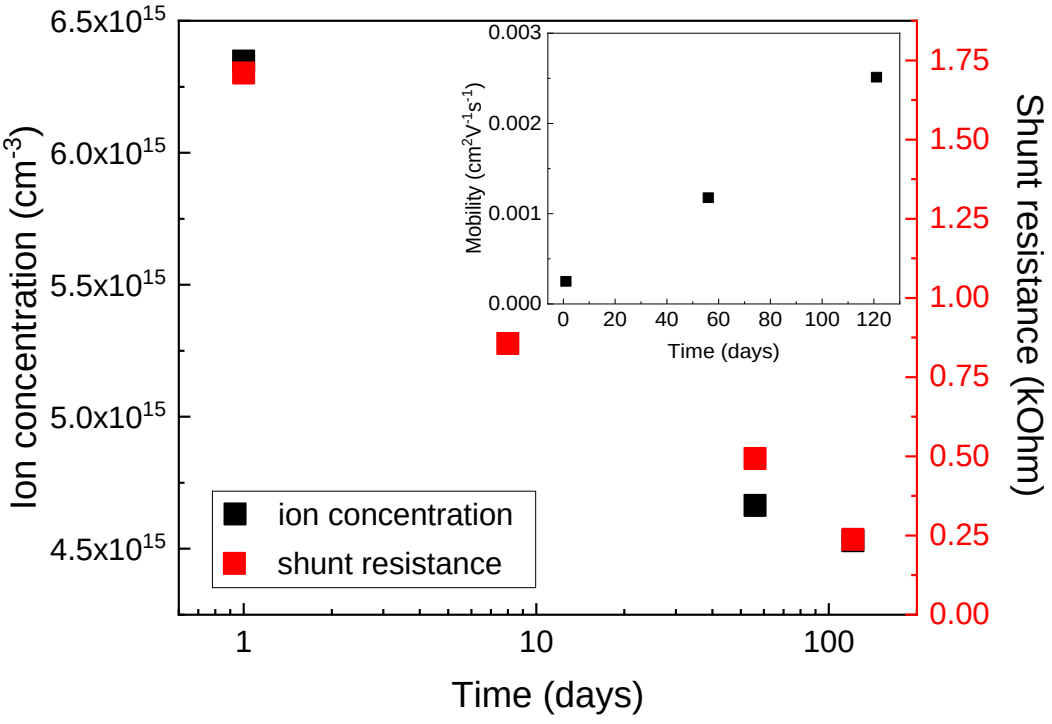

Figure 6. Evolution of estimated mobile ion concentrations with time (left axis) and changes in the cell's shunt resistance (right axis). The inset includes the change of the estimated ion mobility with time.

Theoretical calculations of the diffusion parameters of iodine ions show a variety of activation energies for V_I/V_I^+ vacancy migration, ranging from 0.08 eV [21] to 0.58 eV [25]. Haruyama et al. [39] theoretically calculated the activation energies for different migration paths in $MAPbI_3$ and showed that two migration paths for I^- anions are dominant: in the <100> and <111> direction. According to their work, the activation energy is lowered, from 0.44 eV to 0.33 eV, when I^- ions change the diffusion path from the <100> to <111> plane. Meloni et al. [26] obtained similar theoretical values of 0.45 eV and 0.28 eV, respectively, and linked them to processes responsible for the hysteresis present in the I-V characteristics. Change in the migration path is one of the possible mechanisms responsible for the change in activation energy. The other possibilities are linked to the Meyer-Neldel rule [40] also observed in perovskite solar cells [20], resulting in the relation between the preexponential factor D_0 and the activation energy E_a in Equation (4). Two mechanisms were proposed in perovskite solar cells that may account for the Meyer-Neldel behavior. First relates to the energy distribution in hopping energies [41], which should evolve with time to lower the activation. The second considers a multiphonon excitation model, including the entropy factor in preexponential factor D_0 [42]. In this model, the Meyer-Neldel rule originates from variations in the number of phonons interacting during the ion hopping. The greater the number of interacting phonons, the greater the amount of energy is delivered therefore the lowering of activation energy would take place when less phonons would interact during a single hopping event.

On the other hand, not only anions can migrate in the perovskite material, but the theoretical values for the activation energies of cations, which are also considered to diffuse in perovskites are significantly larger, varying from around 0.8 eV [21][26] to 2.3 eV [25]. This is outside the range of activation energy values observed in our study, except from one of the DLTS signals having an activation energy of around 1.2 eV. The summary of the experimental activation energies is shown in Table 2.

Table 2. Summary of activation energies obtained by AS and DLTS.

Label	Experimental
AS	0.45 ± 0.03 eV
AS degradation	0.37 ± 0.03 eV
DLTS 1	0.56 ± 0.05 eV
DLTS 2	1.21 ± 0.12 eV

4. Conclusions

The AS and DLTS results show that the signals observed in the $FAPbI_3$-based cells using capacitance-based methods relate to ion migration rather than being a response from deep energy levels introduced by a defect. The main arguments supporting this hypothesis are the

observation of large capacitance transients at +1 V, the fact that the process with the same activation energy is visible both at +1 V and 0 V, and the activation energy values by itself. We have tentatively attributed observed signals to anion (AS and DLTS signals with $E_a < 0.56$ eV) and cation (DLTS signal with E_a=1.21 eV) migration. The calculated activation energies and comparison with theoretical calculations support this hypothesis, suggesting that the migration of anions initially occurs mainly in the <100> direction and, with time, changes towards the <111> direction. This change may relate to a decrease in the activation energy and a consequent increase in the ion migration rate, increasing the solar cell's leakage current and decreasing the efficiency.

5. Acknowledgements

This work was supported by the Warsaw University of Technology in the framework of the IDUB-POB-EnergyTech-1 project. JD and EU acknowledge funding from the German Ministry of Education and Research (BMBF) for the Young Investigator Group Hybrid Materials Formation and Scaling (HyPerFORME) within the program "NanoMatFutur" (grant no. 03XP0091) and the "SNaPSHoTs" project (grant no. 01IO1806).

6. References

[1] NREL Best research-cell efficiency chart. Accessed 15 July 2021 (2021)., (n.d.).

[2] M.J.P. Alcocer, T. Leijtens, L.M. Herz, A. Petrozza, H.J. Snaith, Electron-Hole Diffusion Lengths Exceeding Trihalide Perovskite Absorber, Science 342 (2013) 341–344. doi:10.1126/science.1243982.

[3] S.H. Turren-Cruz, M. Saliba, M.T. Mayer, H. Juárez-Santiesteban, X. Mathew, L. Nienhaus, W. Tress, M.P. Erodici, M.J. Sher, M.G. Bawendi, M. Grätzel, A. Abate, A. Hagfeldt, J.P. Correa-Baena, Enhanced charge carrier mobility and lifetime suppress hysteresis and improve efficiency in planar perovskite solar cells, Energy Environ. Sci. 11 (2018) 78–86. doi:10.1039/c7ee02901b.

[4] S. De Wolf, J. Holovsky, S.J. Moon, P. Löper, B. Niesen, M. Ledinsky, F.J. Haug, J.H. Yum, C. Ballif, Organometallic halide perovskites: Sharp optical absorption edge and its relation to photovoltaic performance, J. Phys. Chem. Lett. 5 (2014) 1035–1039. doi:10.1021/jz500279b.

[5] A.M. Askar, K. Shankar, Exciton binding energy in organic-inorganic tri-halide perovskites, J. Nanosci. Nanotechnol. 16 (2016) 5890–5901. doi:10.1166/jnn.2016.12936.

[6] D.L. Losee, Admittance spectroscopy of impurity levels in Schottky barriers, J. Appl. Phys. 46 (1975) 2204–2214.

[7] D. V. Lang, Deep-level transient spectroscopy: A new method to characterize traps in semiconductors, J. Appl. Phys. 45 (1974) 3023–3032. doi:10.1063/1.1663719.

[8] A.S. Gudovskikh, J.P. Kleider, Capacitance spectroscopy of amorphous/crystalline silicon heterojunction solar cells at forward bias and under illumination, Appl. Phys. Lett. 90 (2007) 29–31. doi:10.1063/1.2431783.

[9] A. Urbaniak, K. Macielak, M. Igalson, P. Szaniawski, M. Edoff, Defect levels in

Cu(In,Ga)Se2 studied using capacitance and photocurrent techniques, J. Phys. Condens. Matter. 28 (2016). doi:10.1088/0953-8984/28/21/215801.
[10] M. Burgelman, P. Nollet, Admittance spectroscopy of thin film solar cells, Solid State Ionics. 176 (2005) 2171–2175. doi:10.1016/j.ssi.2004.08.048.
[11] J.M. Frost, A. Walsh, What Is Moving in Hybrid Halide Perovskite Solar Cells?, Acc. Chem. Res. 49 (2016) 528–535. doi:10.1021/acs.accounts.5b00431.
[12] A.Y. Alsalloum, B. Turedi, K. Almasabi, X. Zheng, R. Naphade, S.D. Stranks, O.F. Mohammed, O.M. Bakr, 22.8%-Efficient single-crystal mixed-cation inverted perovskite solar cells with a near-optimal bandgap, Energy Environ. Sci. 14 (2021) 2263–2268. doi:10.1039/d0ee03839c.
[13] D.P. Mcmeekin, G. Sadoughi, W. Rehman, G.E. Eperon, M. Saliba, M.T. Hörantner, A. Haghighirad, N. Sakai, L. Korte, B. Rech, M.B. Johnston, L.M. Herz, H.J. Snaith, A mixed-cation lead mixed-halide perovskite absorber for tandem solar cells, Science 351 (2016) 151–155.
[14] W. Rehman, D.P. McMeekin, J.B. Patel, R.L. Milot, M.B. Johnston, H.J. Snaith, L.M. Herz, Photovoltaic mixed-cation lead mixed-halide perovskites: Links between crystallinity, photo-stability and electronic properties, Energy Environ. Sci. 10 (2017) 361–369. doi:10.1039/c6ee03014a.
[15] K.E. Gkini, M. Antoniadou, N. Balis, A. Kaltzoglou, A.G. Kontos, P. Falaras, Mixing cations and halide anions in perovskite solar cells, Mater. Today Proc. 19 (2019) 73–78. doi:10.1016/j.matpr.2019.07.660.
[16] B. Rivkin, P. Fassl, Q. Sun, A.D. Taylor, Z. Chen, Y. Vaynzof, Effect of Ion Migration-Induced Electrode Degradation on the Operational Stability of Perovskite Solar Cells, ACS Omega 3 (2018) 10042–10047. doi:10.1021/acsomega.8b01626.
[17] D.A. Jacobs, Y. Wu, H. Shen, C. Barugkin, F.J. Beck, T.P. White, K. Weber, K.R. Catchpole, Hysteresis phenomena in perovskite solar cells: The many and varied effects of ionic accumulation, Phys. Chem. Chem. Phys. 19 (2017) 3094–3103. doi:10.1039/c6cp06989d.
[18] J.W. Rosenberg, M.J. Legodi, Y. Rakita, D. Cahen, M. Diale, Laplace current deep level transient spectroscopy measurements of defect states in methylammonium lead bromide single crystals, J. Appl. Phys. 122 (2017). doi:10.1063/1.4995970.
[19] M. Samiee, S. Konduri, B. Ganapathy, R. Kottokkaran, H.A. Abbas, A. Kitahara, P. Joshi, L. Zhang, M. Noack, V. Dalal, Defect density and dielectric constant in perovskite solar cells, Appl. Phys. Lett. 105 (2014). doi:10.1063/1.4897329.
[20] S. Reichert, Q. An, Y.W. Woo, A. Walsh, Y. Vaynzof, C. Deibel, Probing the ionic defect landscape in halide perovskite solar cells, Nat. Commun. 11 (2020). doi:10.1038/s41467-020-19769-8.
[21] J.M. Azpiroz, E. Mosconi, J. Bisquert, F. De Angelis, Defect migration in methylammonium lead iodide and its role in perovskite solar cell operation, Energy Environ. Sci. 8 (2015) 2118–2127. doi:10.1039/c5ee01265a.
[22] M.H. Futscher, J.M. Lee, L. McGovern, L.A. Muscarella, T. Wang, M.I. Haider, A.

Fakharuddin, L. Schmidt-Mende, B. Ehrler, Quantification of ion migration in CH3NH3PbI3 perovskite solar cells by transient capacitance measurements, Mater. Horizons. 6 (2019) 1497–1503. doi:10.1039/c9mh00445a.

[23] W.J. Yin, T. Shi, Y. Yan, Unusual defect physics in CH3NH3PbI3 perovskite solar cell absorber, Appl. Phys. Lett. 104 (2014). doi:10.1063/1.4864778.

[24] A. Senocrate, T.Y. Yang, G. Gregori, G.Y. Kim, M. Grätzel, J. Maier, Charge carrier chemistry in methylammonium lead iodide, Solid State Ionics. 321 (2018) 69–74. doi:10.1016/j.ssi.2018.03.029.

[25] C. Eames, J.M. Frost, P.R.F. Barnes, B.C. O'Regan, A. Walsh, M.S. Islam, Ionic transport in hybrid lead iodide perovskite solar cells, Nat. Commun. 6 (2015) 2–9. doi:10.1038/ncomms8497.

[26] S. Meloni, T. Moehl, W. Tress, M. Franckeviius, M. Saliba, Y.H. Lee, P. Gao, M.K. Nazeeruddin, S.M. Zakeeruddin, U. Rothlisberger, M. Graetzel, Ionic polarization-induced current-voltage hysteresis in CH3NH3PbX3 perovskite solar cells, Nat. Commun. 7 (2016). doi:10.1038/ncomms10334.

[27] J. Dagar, K. Hirselandt, A. Merdasa, A. Czudek, R. Munir, F. Zu, N. Koch, T. Dittrich, E.L. Unger, Alkali Salts as Interface Modifiers in n-i-p Hybrid Perovskite Solar Cells, Sol. RRL. 3 (2019) 1–10. doi:10.1002/solr.201900088.

[28] J. Li, J. Dagar, O. Shargaieva, M.A. Flatken, H. Köbler, M. Fenske, C. Schultz, B. Stegemann, J. Just, D.M. Többens, A. Abate, R. Munir, E. Unger, 20.8% Slot-Die Coated MAPbI3 Perovskite Solar Cells by Optimal DMSO-Content and Age of 2-ME Based Precursor Inks, Adv. Energy Mater. 2003460 (2021). doi:10.1002/aenm.202003460.

[29] J. Dagar, M. Fenske, A. Al-Ashouri, C. Schultz, B. Li, H. Köbler, R. Munir, G. Parmasivam, J. Li, I. Levine, A. Merdasa, L. Kegelmann, H. Näsström, J.A. Marquez, T. Unold, D.M. Többens, R. Schlatmann, B. Stegemann, A. Abate, S. Albrecht, E. Unger, Compositional and Interfacial Engineering Yield High-Performance and Stable p-i-n Perovskite Solar Cells and Mini-Modules, ACS Appl. Mater. Interfaces. (2021). doi:10.1021/acsami.0c17893.

[30] W. Shockley, W.T. Read, Statistics of Recombination of Holes and Electrons, Phys. Rev. 87 (1952) 835–842.

[31] T. Eisenbarth, T. Unold, R. Caballero, C.A. Kaufmann, H. Schock, T. Eisenbarth, T. Unold, R. Caballero, C.A. Kaufmann, Interpretation of admittance, capacitance-voltage, and current-voltage signatures in Cu(In ,Ga)Se2 thin film solar cells., J. Appl. Phys. 107 (2010). doi:10.1063/1.3277043.

[32] U. Reislöhner, H. Metzner, C. Ronning, Hopping conduction observed in thermal admittance spectroscopy, Phys. Rev. Lett. 104 (2010) 2–5. doi:10.1103/PhysRevLett.104.226403.

[33] A. Rohatgi, S.K. Pang, The deep level transient spectroscopy studies of a ZnO varistor as a function of annealing, J. Appl. Phys. 5375 (1988) 5375–5379.

[34] A. Sehpar, S. Paek, A.Y. Polyakov, N.B. Smirnov, I. V Shchemerov, D.S. Saranin, S.I. Didenko, Z. Ahmad, F. Touati, Solar Energy Materials and Solar Cells Assessing mobile

ions contributions to admittance spectra and current-voltage characteristics of 3D and 2D / 3D perovskite solar cells, Sol. Energy Mater. Sol. Cells. 215 (2020) 110670. doi:10.1016/j.solmat.2020.110670.

[35] G.H. Vineyard, Frequency factors and isotope effects in solid state rate processes, J. Phys. Chem. Solids. 3 (1957) 121–127. doi:10.1016/0022-3697(57)90059-8.

[36] D. Ware, P. Mansfield, High stability “boxcar” integrator for fast NMR transients in solids, Rev. Sci. Instrum. 37 (1966) 1167–1171. doi:10.1063/1.1720449.

[37] W.S. Yang, B.W. Park, E.H. Jung, N.J. Jeon, Y.C. Kim, D.U. Lee, S.S. Shin, J. Seo, E.K. Kim, J.H. Noh, S. Il Seok, Iodide management in formamidinium-lead-halide-based perovskite layers for efficient solar cells, Science 356 (2017) 1376–1379. doi:10.1126/science.aan2301.

[38] C.E. Michelson, A. V. Gelatos, J.D. Cohen, Drive-level capacitance profiling: Its application to determining gap state densities in hydrogenated amorphous silicon films, Appl. Phys. Lett. 47 (1985) 412–414. doi:10.1063/1.96129.

[39] J. Haruyama, K. Sodeyama, L. Han, Y. Tateyama, First-principles study of ion diffusion in perovskite solar cell sensitizers, J. Am. Chem. Soc. 137 (2015) 10048–10051. doi:10.1021/jacs.5b03615.

[40] H. Meyer, W and Neldel, Relation between the energy constant and the quantity constant in the conductivity--temperature formula of oxide semiconductors, Z. Tech. Phys. 18 (1937) 588–593.

[41] R. Metselaar, G. Oversluizen, The meyer-neldel rule in semiconductors, J. Solid State Chem. 55 (1984) 320–326. doi:10.1016/0022-4596(84)90284-6.

[42] A. Yelon, B. Movaghar, Microscopic explanation of the compensation (Meyer-Neldel) rule, Phys. Rev. Lett. 65 (1990) 618–620. doi:10.1103/PhysRevLett.65.618.